

# Theory of Dike Intrusion in a Saturated Porous Solid

DEREK ELSWORTH

*Department of Mineral Engineering, Pennsylvania State University, University Park*

BARRY VOIGHT

*Department of Geosciences, Pennsylvania State University, University Park*

A study of the pore pressure fields that develop around intruding dikes is described under the motivation that intruded geometry may be determined from pore pressures recorded in relatively remote monitoring wells. The pore pressure fields induced around cylindrical and planar intrusions are described as analogues to moving point or line dislocations within an infinite saturated porous elastic medium. The resulting transient pressure fields reduce to an equivalent steady state when viewed from the advancing front. Solutions for the moving point and line dislocations yield a dependence on common dimensionless groupings. Thus, dimensionless pressure rise accompanying intrusion, and recorded at a static location, may be uniquely referenced to the dimensionless parameters representing emplacement velocity and time. The resulting transient pressure response may be divided into two groups, representing fast and slow emplacement. Where hydraulic parameters representing the host porous medium are known a priori, both emplacement location and the cross-sectional area may be determined uniquely. For slow emplacement, the intrusion rate may also be determined; only a lower limiting intrusion rate may be discerned for fast emplacement. Field data are rare, but two intrusive events at Krafla, Iceland are examined using the proposed moving dislocation models. Predicted location and lower limiting intrusion rate of the Krafla dikes compare favorably with field observation despite more than a 9 km separation to the monitoring well.

## INTRODUCTION

Knowledge of the magma ascent rate is required for a proper understanding of volcanic systems and eruption processes and is important for eruption prediction [Kushiro, 1980; Turcotte, 1982; Ida and Kumazawa, 1986; Chadwick et al., 1988; Shimozuro, 1989]. Despite this significance, the determination of ascent rates has remained historically elusive, as few volcanoes are adequately instrumented to determine magma migration [Endo et al., 1990]. In the following, an appraisal is made of the suitability of using pore pressure increases to determine both the morphology and emplacement rate of magmatic intrusions.

Magmatic emplacement results in a sudden volumetric increase within the saturated medium [Turcotte, 1990], with secondary volumetric changes possibly resulting from thermal expansion within the saturated porous medium surrounding the intrusion [Delaney, 1982; Watanabe, 1983]. Together, these processes result in an instantaneous change in pore fluid pressures around the location of emplacement. Although data documenting these processes are rare, two events at Krafla, Iceland have supplied relatively complete transient pore pressure records recorded in a single well. The rapid pressure rise and subsequent slow pressure drop measured in a single well at the Krafla geothermal site may be used to infer the path of magma ascent within the host rock. Indeed, if the processes describing changes in pore pressure that result from intrusion are sufficiently quantified, a surprising array of parameters describing dike morphology may be ascertained. The possibility of inferring dike morphology, from pore pressures recorded at a single location in the surrounding medium, is developed in the following.

Copyright 1992 by the American Geophysical Union.

Paper number 92JB00519.  
0148-0227/92/92JB-00519\$05.00

Undrained changes in pore pressure may be represented by the concept of a dilation center [Cleary, 1977]. For a migrating dilation center representing the continuous intrusion process, the resulting pore pressure field may be represented by a succession of dilation centers to reproduce appropriate boundary conditions. Boundary conditions at the interface between the intrusion and the host rock may be applied as either stress-free [Cleary, 1978] or displacement conditions [Elsworth, 1991], with the latter proving most convenient for this particular type of viscous intrusion. Consequently, moving point and line dislocations may be considered analogous to the bounding geometries of an intruded dike of finite extent. Pore pressure responses within the porous medium surrounding intruded line and sheet dikes are defined in the following as bounding cases. The insensitivity of the pore pressure response to prescribed geometry is apparent in the results.

## POINT DISLOCATION IN A POROELASTIC MEDIUM

The pore pressure field that results from dilation of an infinitesimal cubic volume within a saturated porous elastic medium is available from Cleary [1977]. The point dilation is centered at the origin. The walls of the infinitesimal cube separate exterior and interior problem domains that may be considered independently. Applying an instantaneous but permanent hydrostatic expansion of the interior cube at time  $t=0$  results in a volumetric change of "strength",  $Z$ . Considering the interior problem first, an arrangement of dipole forces are applied to the faces of the cubic volume to yield the required volume change,  $Z$ . The concurrent application of an equal but opposing set of forces to the surface of the exterior medium retains displacement continuity between the exterior and interior domains. The cubic region may be arbitrarily reduced to a point where, by definition, the magnitude of the applied dipole forces remain constant and the strength of the dislocation,  $Z$ , is also retained finite. This application of forces

results in an expansion of the cubic interior volume and is accompanied by a corresponding increase in void volume. In order to retain saturation of this volume and thereby satisfy continuity for the fluid (diffusion equation), an instantaneous fluid source must be supplied at far-field pressure. The superposition of the continuous dipole triplicate and an instantaneous point fluid source of appropriate magnitude give, directly, the pore pressure Green's function for a point normal dislocation in an infinite medium [Cleary, 1977; Rudnicki, 1981] as

$$p - p_s = \frac{KZ}{4\pi R^3} \left[ \frac{B(1+\nu_u)}{3(1-\nu_u)2\sqrt{\pi}} \xi^3 e^{-\frac{\xi^2}{4}} \right] \quad (1)$$

with

$$\xi = \frac{R}{\sqrt{ct}} \quad (2)$$

and

$$R^2 = x^2 + y^2 + z^2 \quad (3)$$

where induced pore pressures,  $p - p_s$ , above ambient pressure,  $p_s$ , are spherically symmetric within the Cartesian  $(x, y, z)$  space. The strength,  $Z$ , of the dislocation is conditioned by the effective modulus of the interior region,  $K$ , whereby the product,  $KZ$ , directly represents the magnitude of the dipole triplicate. The material coefficients are those of undrained Poisson ratio,  $\nu_u$ , that takes the range  $\nu < \nu_u < 0.5$  where  $\nu$  is the drained magnitude [Rice and Cleary, 1976], the consolidation coefficient or synonymous hydraulic diffusivity of the isotropic saturated porous elastic medium,  $c$ , and the Skempton pore pressure parameter,  $B$ , representing the ratio of induced undrained pressure change to mean applied stress [Skempton, 1954].

Since the analysis in the exterior is linearly elastic, pore pressures generated by induced deviatoric total stresses are controlled by the Skempton A parameter, which for a linearly elastic body reduces to  $A=1/3$  [Skempton, 1954]. In equation (1) induced pressures vanish as  $R \rightarrow \infty$  and as  $t \rightarrow \infty$ .

Magma intrusion may be represented as a displacement controlled process. If magma injection rate is prescribed as the primary boundary condition that controls intrusion, then it is more convenient to relate induced pore pressures directly to the dilation volume rather than via the indeterminate magnitude of the dipole strength,  $KZ$ . Total volume change,  $V$ , resulting from a dislocation at the origin is

$$V = \int_{-\infty}^{+\infty} \int_{-\infty}^{+\infty} \int_{-\infty}^{+\infty} (p - p_s) m \, dx \, dy \, dz \quad (4)$$

where the compressibility,  $m$ , of the saturated medium is recovered from the hydraulic diffusivity,  $c$ , intrinsic permeability,  $k$ , and fluid dynamic viscosity,  $\mu$ , as  $m = k/(c\mu)$ . Substituting equation (1) into equation (4) and completing the integration yields

$$KZ = c \frac{\mu}{k} V \frac{3(1-\nu_u)}{B(1+\nu_u)} \quad (5)$$

where  $V$  is constant in time. Resubstituting equation (5) into equation (1) yields the induced pore pressure field that results

from insertion of volume,  $V$ , into the porous medium at time,  $t=0$ , and leaves the cavity inflated at this volume for  $t \geq 0$ . The resulting expression is

$$p - p_s = \frac{cV}{4\pi R^3} \frac{\mu}{k} \frac{\xi^3}{2\sqrt{\pi}} e^{-\frac{\xi^2}{4}} \quad (6)$$

representing the spherically symmetric pore pressure field.

**Moving Point Dislocation**

The point normal dislocation of equation (6) may be readily integrated in time and space to represent a moving or arrested dislocation [Elsworth, 1991] where the fluid and deformation fields of the linear system remain coupled throughout. For a moving dislocation the continuous dislocation volume,  $V$ , is replaced by a volumetric rate and integrated in time and space. For a dislocation of cross-sectional area,  $a$ , moving within the porous medium at velocity,  $U$ , as illustrated in Figure 1, the substitution

$$V = Uad\tau \quad (7)$$

may be used, where  $\tau$  is the discrete parameter of time integration. A moving coordinate system is chosen that migrates in the negative  $x$  direction with the front of the traveling point dislocation. The position of a point located relative to the primary dislocation at coordinates  $(x, y, z)$  at current time  $t$  would have been  $([x-U(t-\tau)], y, z)$  at time  $\tau$ . Substituting equation (7) and the coordinate transform (of equation (9)) into equation (6) and integrating in time ( $\tau$ ) between the time of initiation ( $\tau=0$ ) and the current time ( $\tau=t$ ) gives

$$p - p_s = \frac{cUa}{4\pi} \frac{\mu}{k} \int_0^t \frac{\xi^3}{2\bar{R}^3\sqrt{\pi}} e^{-\frac{\xi^2}{4}} d\tau \quad (8)$$

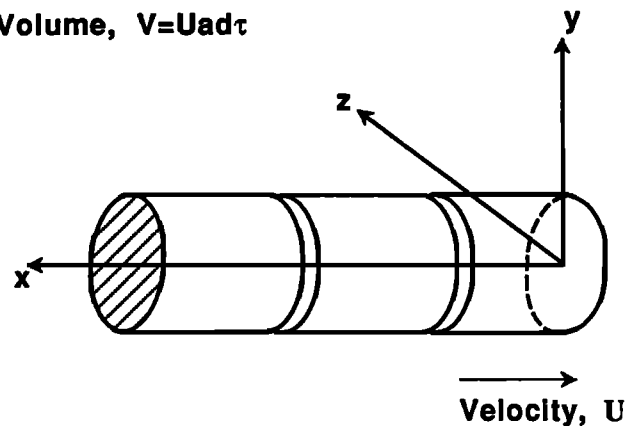
where

$$\bar{R}^2 = [x - U(t - \tau)]^2 + y^2 + z^2 \quad (9)$$

and

$$\xi = \frac{\bar{R}}{\sqrt{ct}} \quad (10)$$

**Volume,  $V=Uad\tau$**



**Cross-sectional area,  $a$**

Fig. 1. Local coordinate system for a moving point dislocation.

Substituting the dummy variable

$$\eta = \frac{R}{2\sqrt{c}(t-\tau)} \tag{11}$$

into equation (8), yields, following some rearrangement,

$$p-p_s = \frac{\mu}{k} \frac{Ua}{2\pi^2 R} e^{\frac{Ux}{2c}} \int_{\frac{R}{2\sqrt{ct}}}^{\infty} e^{-\eta^2 - (\frac{UR}{4c\eta})^2} d\eta \tag{12}$$

where  $R^2 = x^2 + y^2 + z^2$ . The integral must be evaluated numerically except for the steady condition where  $t \rightarrow \infty$  when the pressure distribution reduces to

$$p-p_s = \frac{\mu}{k} \frac{Ua}{4\pi R} e^{-\frac{U(R-x)}{2c}} \tag{13}$$

*Dimensionless parameters.* The pressure response may be viewed in terms of a minimum set of dimensionless parameters. The system may be defined through the dimensionless parameters,

$$P_D = \frac{4\pi l (p-p_s) k}{Ua \mu} \tag{14}$$

$$U_D = \frac{Ul}{2c} \tag{15}$$

$$t_D = \frac{4ct}{l^2} \tag{16}$$

$$(x_D, y_D, z_D) = \frac{1}{l}(x, y, z) \tag{17}$$

$$R_D^2 = x_D^2 + y_D^2 + z_D^2 \tag{18}$$

representing dimensionless pore fluid pressure at the monitoring location,  $P_D$ , dimensionless intrusion velocity,  $U_D$ , dimensionless time,  $t_D$  and dimensionless coordinates  $(x_D, y_D, z_D)$ . Here,  $l$  is introduced as the minimum distance from a pore pressure monitoring location to the path of the dislocation, as illustrated in Figure 2. Rearranging equations (12) and (13) in terms of these dimensionless parameters

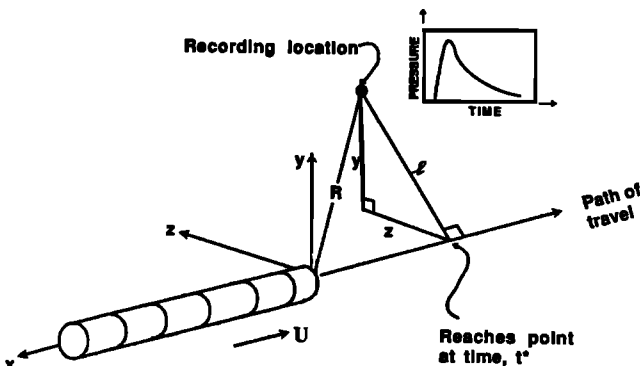


Fig. 2. Local coordinate system for a moving point dislocation relative to a static measuring location.

enables the transient behavior to be defined as

$$P_D R_D = \frac{2}{\sqrt{\pi}} \int_{\frac{R_D}{\sqrt{t_D}}}^{\infty} e^{U_D x_D - \eta^2 - (\frac{U_D R_D}{2\eta})^2} d\eta \tag{19}$$

and the steady behavior to be described as

$$P_D R_D = e^{-U_D (R_D - x_D)} \tag{20}$$

where the maximum magnitude of dimensionless pore pressure,  $P_D$ , is unity. Both equations (19) and (20) are written with reference to the moving coordinate system and must be appropriately transformed to represent the transient response at a static measuring location, adjacent to the migrating dislocation. If time,  $t^*$ , is defined as the time at which the path of the dislocation is closest to the pore pressure measuring location, as identified in Figure 2, then the moving coordinate system may be transformed on noting that

$$x_D = \frac{U}{l}(t-t^*) = \frac{1}{2} U_D (t_D - t_D^*) \tag{21}$$

where

$$t_D^* = \frac{4ct^*}{l^2} \tag{22}$$

enabling dimensionless radius,  $R_D$ , to be defined as

$$R_D^2 = x_D^2 + 1 \tag{23}$$

where it is apparent from Figure 2 that  $y_D^2 + z_D^2 = 1$ . Thus the transient pore pressure response may be fully defined as a migrating dislocation approaches, reaches and ultimately passes a particular location.

*Pressure buildup.* Pressure buildup behavior is of particular use in determining the applicability of the steady state approximation of equation (20) in the analysis of intrusion problems. The true transient behavior is determined from an intrusive event initiating at time,  $t=0$ , and continuing until current time from equation (19). Since the steady condition migrates outwards from the tip of the advancing dislocation, it is only relevant to discuss the steady state relative to the moving coordinate system.

In determining the closeness to the steady state it is desired to compare pressure at any time level with the steady magnitude of  $P_D R_D$ . According to equation (19), representing the full transient behavior, the maximum set of dimensionless parameters describing the system are

$$P_D R_D = f \left[ \frac{t_D}{R_D^2}; U_D x_D; U_D \right] \tag{24}$$

For small  $U_D x_D$  the behavior of the integral is asymptotic to a threshold response in terms of dimensionless time,  $t_D/R_D^2$  [see Elsworth, 1991]. Thus, for  $U_D x_D < 10^{-2}$  the time to reach 95% of the steady pressure at any location around the advancing dislocation front is given by

$$\frac{t_D}{R_D^2} = 500 \quad \text{for } U_D x_D \leq 10^{-2} \tag{25}$$

As magnitudes of  $U_D x_D$  increase the pressure response time and duration are simultaneously reduced. The time to steady response may be approximated by the inflection point of the  $P_D R_D$  versus  $t_D/R_D^2$  curve [Elsworth, 1991] and is appropriately given by

$$\frac{\partial^2(P_D R_D)}{\partial \eta^2} = 0 \tag{26}$$

or

$$\frac{t_D}{R_D^2} = \frac{2}{U_D R_D} \quad \text{for } U_D x_D \geq 10^1 \tag{27}$$

The asymptotic values of equations (25) and (27) enable the suitability of using the approximate steady representation to be determined. Knowledge of the measuring location relative to the intruded feature enables an evaluation of the appropriateness to be made provided material parameters are available for the host porous medium. The quasi-steady approximation of equation (20) yields a suitable approximation in many instances, as evidenced in the observed fit between theory and experiment, presented later.

**Steady pressure distribution.** After relatively small penetration distances the pressure distribution surrounding the tip of an advancing dislocation is well approximated by the steady representation of equation (20). Although the pressure distribution is steady relative to the moving coordinate frame, a recording location fixed in space will register a transient response as the perturbation approaches. The pressure response relative to the moving coordinate system may be transformed to the time domain on substitution of equations (21) and (23) into equation (20). In this procedure the time frame is referenced to that when the path of the dislocation passes closest at  $t^*$ , as illustrated in Figure 2. Through this transform, only three independent parameters remain in equation (20), namely,

$$P_D = f[U_D, U_D(t_D - t_D^*)]. \tag{28}$$

The pressure changes that occur as a moving dislocation approaches and subsequently departs the measuring location may be illustrated separately in Figures 3 and 4, respectively, where equations (21) through (23) are substituted into equation (20). Where the dislocation approaches at low velocity,  $U_D$ , the

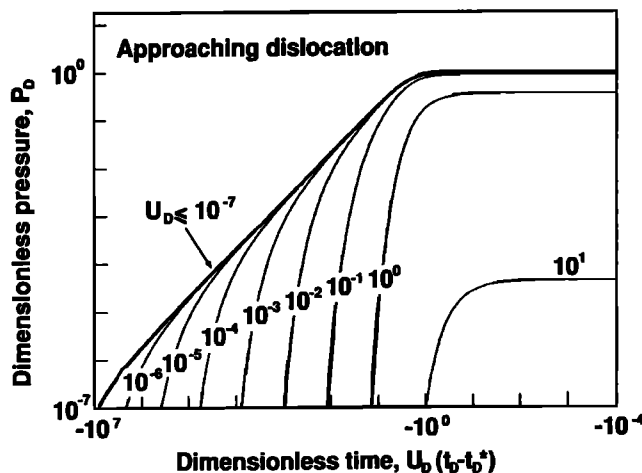


Fig. 3. Dimensionless pore pressure versus dimensionless time resulting from an approaching point dislocation.

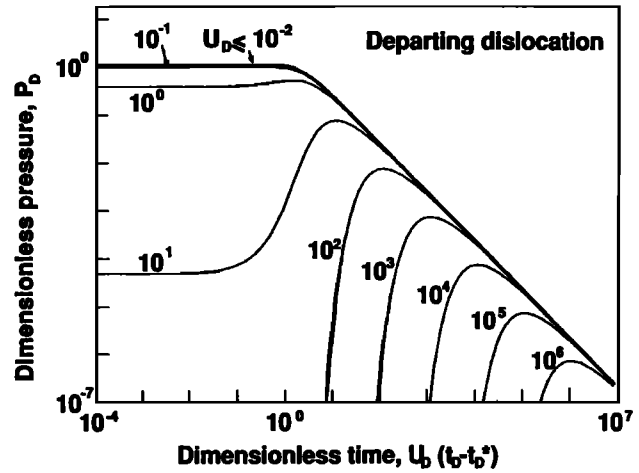


Fig. 4. Dimensionless pore pressure versus dimensionless time resulting from a departing point dislocation.

diffusive augmentation of pore fluid pressures at the measuring location occurs at a rate consistent with migration of the dislocation, as illustrated in Figure 3. As the dislocation velocity increases, pressure buildup is no longer able to keep up with the moving dislocation front. Consequently, for  $U_D > 10^0$ , the induced pore pressures have not yet reached a peak even when the dislocation front is in the closest location at  $t^*$  represented by  $U_D(t_D - t_D^*) = 0$ .

The pore pressures generated after the dislocation passes the measuring location are illustrated in Figure 4. Clearly visible is the lag to peak pressure for large magnitudes of dimensionless dislocation velocity,  $U_D$ . For small velocities, the peak pressure is reached concurrently with the dislocation approaching the measuring location and a symmetry is noted with the prepeak transient record. The symmetry of the transient record is indicative of the spherical pressure distribution evident around the advancing dislocation as noted elsewhere [Elsworth, 1991]. As dimensionless dislocation velocity increases, the spherical distribution is flattened ahead of the dislocation front, resulting in the characteristic delay apparent in Figure 4.

Although useful to understand the processes accompanying pore pressure generation around a migrating dislocation, the use of the parameter  $U_D(t_D - t_D^*)$  is not practical for the reduction of field data. Clearly, the time at which the dislocation passes closest to the measuring location,  $t^*$  (i.e., when the physical separation is  $l$ ), is not generally available and must be substituted by a field discernible parameter. The peaked form of the pressure response is evident from equation (20), where the appropriate substitution of equations (21) through (23) is made. When pore pressures are plotted relative to prepassage and postpassage times, as illustrated in Figures 3 and 4, the logarithmic time scale masks the true peaked nature of the response. Referencing both field data and analytical solutions relative to the time to peak pore fluid pressure,  $t^P$ , enables a common reference frame to be established. Correspondingly, the time to peak pressure may be evaluated by differentiating equation (20) with respect to  $x_D$  and setting the result to zero. This yields the relation

$$U_D = \frac{\left(\frac{x_D^P}{R_D}\right)^2}{\left(1 - \frac{x_D^P}{R_D}\right)x_D} \tag{29}$$

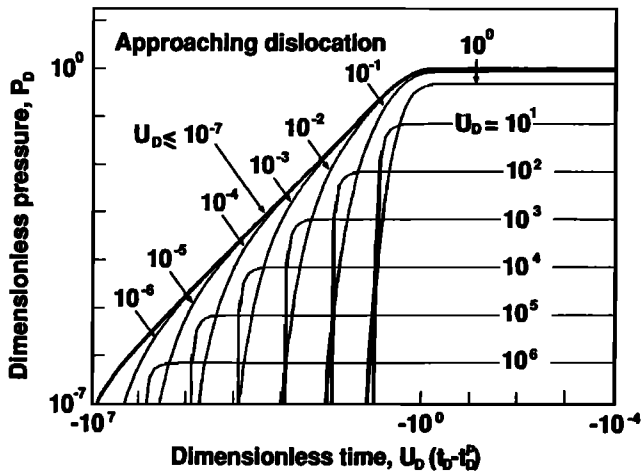


Fig. 5. Dimensionless pore pressure versus dimensionless time resulting from an approaching point dislocation relative to time to peak pressure.

where the p superscript refers to the magnitudes of  $x_D$ ,  $R_D$  and  $t_D$  at peak pore fluid pressure. Pore pressure transients may therefore be evaluated relative to the peak as illustrated in Figures 5 and 6 for the prepeak and postpeak regimes, respectively. As expected, the symmetric form of the response for small  $U_D$  is little affected. For large dislocation velocities an asymmetric form to the response is apparent in the translated configuration. An extremely rapid pressure increase is apparent as the dislocation approaches, representing the undrained loading applied to the system.

Presentation of the data in the form of Figures 5 and 6 enables direct reduction of field data, since time to peak pressure may be directly discerned.

**Pressure decay following termination.** For a dislocation that terminates close to the measuring location, pressure response may be determined from the full transient representation of equation (19). Superposition is used to represent termination that occurs at time  $t'$ , prior to the current time level of interest,  $t$ . A continuous dilational dislocation is introduced spanning  $0 < \tau < t$ , and a second contractile dislocation of equal but opposite magnitude is applied in the interval  $t' < \tau < t$ . This

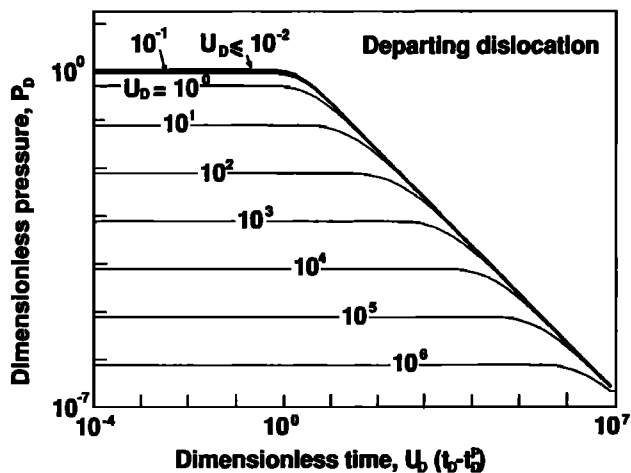


Fig. 6. Dimensionless pore pressure versus dimensionless time resulting from a departing point dislocation relative to time to peak pressure.

system of concurrent dislocations is represented as

$$P_D R_D = \frac{2}{\sqrt{\pi}} e^{U_D R_D} \int_{\frac{R_D}{\sqrt{t_D}}}^{\frac{R_D}{\sqrt{t_D - t'}}} e^{-\eta^2 - (\frac{U_D R_D}{2\eta})^2} d\eta \quad (30)$$

where

$$t'_D = \frac{4ct'}{l^2} \quad (31)$$

and pressures must be referenced back to the coordinate system, arrested at time  $t'$ , through

$$x = x' - U(t - t'); y = y'; z = z' \quad (32)$$

where the prime represents coordinates relative to the arrested geometry. In dimensionless form, these can be retransformed as

$$x_D = x'_D + \frac{1}{2} U_D (t_D - t'_D) \quad (33)$$

enabling pore pressure dissipation to be determined around the terminated dislocation. Although useful for completeness, the expressions for pressure dissipation around the dislocation are of limited use in the reverse analysis of poorly defined systems due primarily to uniqueness requirements. The interested reader is referred elsewhere [Elsworth, 1991] to explore trends resulting from pressure dissipation. The analyses of most use in the following data reduction are those representing the steady condition.

### Moving Line Dislocation

For unsteady, steady and terminated line dislocations, linear superposition of the pressure distributions previously defined in equations (19), (20) and (30) for point dislocations may be used where St. Venant's principle is assumed. Similarly, this principle holds in determining the applicability of the quasi-steady approximation to a nominally transient process. Alternatively, the pressure transient behavior may be formally evaluated for a limiting case to examine the anticipated variation in response between a point dislocation and a line dislocation of infinite extent. The modified geometry is illustrated in Figure 7 for a dislocation of infinite extent in the y direction, comprising a planar intrusion.

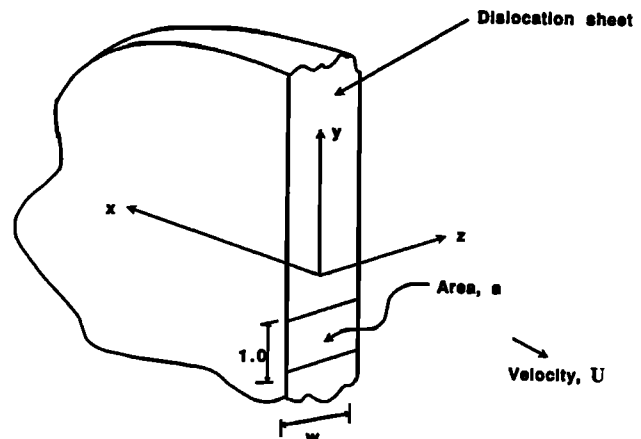


Fig. 7. Local coordinate system for a moving line dislocation.

The steady pressure response around the tip of an advancing line dislocation may be obtained by replacing the cross-sectional area of the dislocation,  $a$ , by the area per unit length in the  $y$ -direction,  $w$ , as illustrated in Figure 7. Substituting  $a=wdy$  into equation (13), and representing a feature of infinite extent in the  $y$  direction yields

$$p^l - p_s = \frac{\mu}{k} \frac{Uw}{4\pi} \int_{-\infty}^{+\infty} \frac{1}{(x^2+z^2+y^2)^{3/2}} e^{-\frac{U((x^2+z^2+y^2)^{1/2}-x)}{2c}} dy \quad (34)$$

resulting in

$$P_D^l = K_0[U_D R_D] e^{U_D x_D} \quad (35)$$

where  $K_0[x]$  is the modified Bessel function of the second kind of order zero and all dimensionless parameters are as previously defined in equations (15) through (18), excepting dimensionless pressure. Dimensionless pore pressure for the line dislocation is now represented as

$$P_D^l = \frac{2\pi(p^l - p_s) k}{Uw \mu} \quad (36)$$

Comparing dimensionless pore pressures for the point and line dislocations (equations (14) and (36)), it is apparent that length to the measuring location,  $l$ , has been replaced in lieu of intruded width,  $w$ , to retain the correct dimensionality of the parameter. Similar to the previous case, the steady distribution around the advancing tip may be transformed using equations (21) and (23) to yield the transient behavior observed at a static recording location. The pressure behavior relative to the time of dislocation passage,  $t^*$ , is documented in Figures 8 and 9. As a result of the differing geometry of the intrusion, dimensionless pressure magnitudes are not limited by unity. As the dislocation approaches, a steep pressure rise is exhibited for increasing magnitudes of intrusion or penetration rate,  $U_D$ , as apparent in Figure 8. When represented in log time, the steep pressure rise is masked by the stretching of the horizontal axis, especially at times close to the peak. The peak dimensionless pore pressure magnitude resulting from the line dislocation increases with a decrease in dimensionless intrusion or penetration rate,  $U_D$ , but real pressures increase even more rapidly due to the inverse

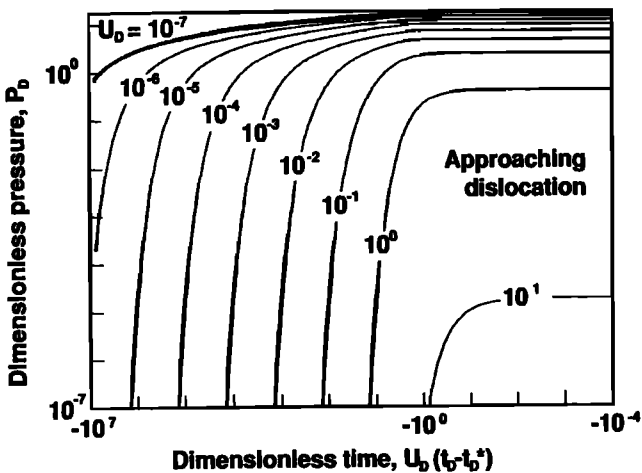


Fig. 8. Dimensionless pore pressure versus dimensionless time resulting from an approaching line dislocation.

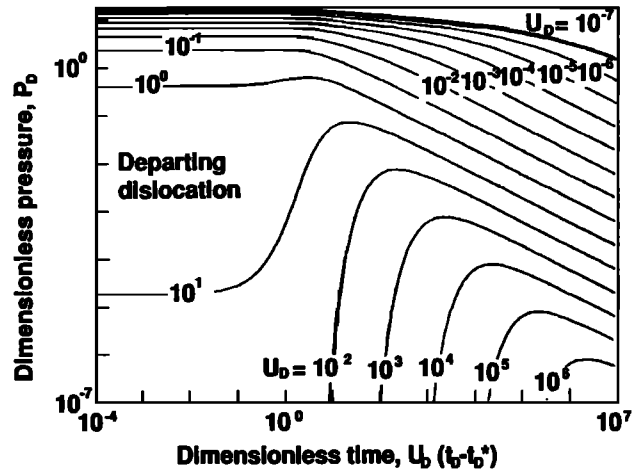


Fig. 9. Dimensionless pore pressure versus dimensionless time resulting from a departing line dislocation.

dependence on penetration rate,  $U$ , apparent from equation (36).

Induced pressures postpassage of the dislocation are less sharply peaked than for the point dislocation, reflecting the different geometry of the dislocations. A mild peak is evident as  $U_D$  increases above unity, as apparent in Figure 9.

For large  $U_D R_D$  the Bessel function of equation (35) may be approximated by an exponential form as  $K_0[x] \approx \sqrt{\pi}/2x e^{-x}$ . Substituting the approximation for  $U_D R_D > 10^1$  yields

$$P_D^l = \frac{\sqrt{\pi}}{\sqrt{2U_D R_D}} e^{-U_D (R_D - x_D)} \quad (37)$$

The similarity between this expression and that for a point dislocation, represented in equation (20), may be noted.

To enable data reduction, the pressure transient records must be evaluated relative to time to peak pore pressure,  $t^P$ . Using equation (35) to evaluate

$$\frac{\partial P_D}{\partial x_D} = 0 \quad (38)$$

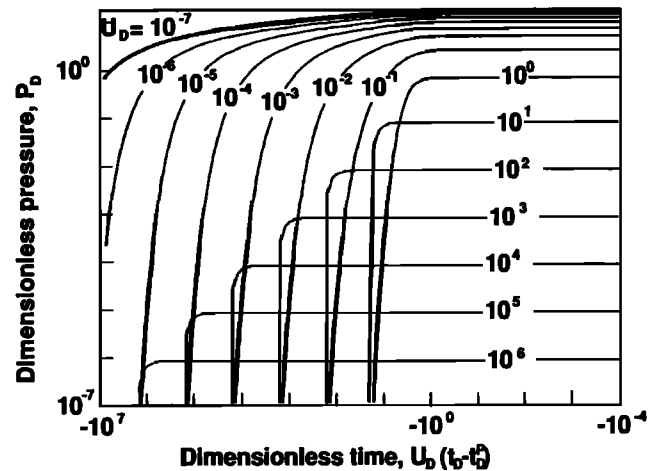


Fig. 10. Dimensionless pore pressure versus dimensionless time resulting from an approaching line dislocation relative to the time to peak pressure.

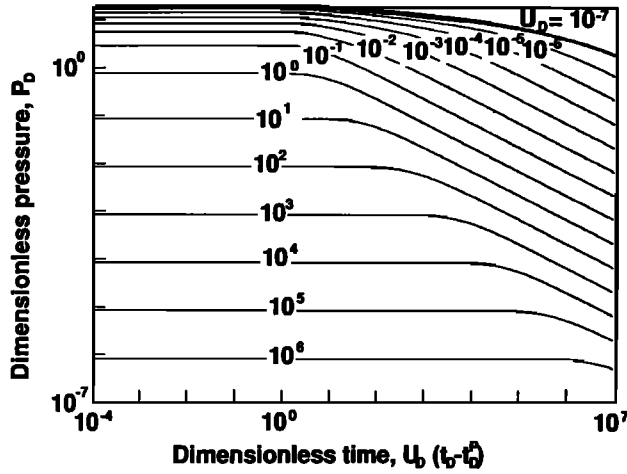


Fig. 11. Dimensionless pore pressure versus dimensionless time resulting from a departing line dislocation relative to the time to peak pressure.

yields

$$\frac{K_0[U_D R_D]}{K_1[U_D R_D]} = \frac{x_\beta}{R\beta} \quad (39)$$

where  $R\beta$  is a unique function of  $x_\beta$ , as apparent from equation (23), and  $K_1[x]$  is the modified Bessel function of the second kind of order one. Following directly from equation (39), the pressure response may be determined relative to time to peak pressure,  $t_\beta$ , as illustrated in Figures 10 and 11.

The prepeak pressure rise steepens with increased dimensionless penetration rate,  $U_D$ , enabling a unique fit to be attempted for  $U_D < 10^0$ , as apparent in Figure 10. This differentiation holds in the postpeak regime, where different transient responses are apparent for  $U_D < 10^0$  in Figure 11.

#### TYPE CURVE DATA REDUCTION

In evaluating field-recorded response, different data reduction procedures must be applied for data recorded in the two families of  $U_D > 10^0$  and  $U_D < 10^{-1}$ . The behavior for data within these two separate families is, not surprisingly, similar for the point and line dislocations. The similarities in behavior result from the line dislocation system being linked to the point source system through linear superposition or equivalent integration.

In all attempts to provide a match, prepeak and postpeak pressure data must be used with the corresponding type curves of Figures 5 and 6 for the point dislocation and Figures 10 and 11 for the line dislocation. The curves must be matched simultaneously to provide identical match points in terms of pressure and time on the two plots.

#### Point Dislocation for $U_D > 10^0$

The similarity between the curves in the postpeak pressure regime (Figures 5 and 6) is such that multiple matches may be made to yield matching pairs of  $P_D$  and  $U_D(t_D - t_\beta)$  for any fitted magnitude of  $U_D$ . However, the behavior is such that the product  $U_D(t - t_\beta)$ , in units of time, is constant for any  $U_D$ .

An arbitrary match point may be chosen, the most convenient one being  $U_D(t_D - t_\beta) = 10^0$ . This enables the minimum distance to the measuring location,  $l$ , to be determined from

$$l = \sqrt{U_D(t - t_\beta)} \sqrt{Ac} \quad (40)$$

where it is assumed that the hydraulic diffusivity,  $c$ , is known a priori. Although this is the most likely situation with hydraulic diffusivity determined from relatively simple field testing, in certain instances the intrusive geometry may be well defined, and diffusivity may be verified against equation (40).

In the range  $U_D > 10^0$ , it is apparent from Figures 5 and 6 that the product  $U_D P_\beta$  is constant and is given approximately by  $U_D P_\beta = 0.74$ . This limit may be discerned directly from equation (20) and noting that for large  $U_D x_D$ , equation (27) yields the relation  $2x_\beta \approx U_D$ . Since large  $U_D$  implies large  $x_D$ , then  $R_D \approx x_D$  and substituting into equation (20) gives

$$U_D P_\beta \approx 2e^{-1} \approx 0.7358 \quad (41)$$

With this product defined, peak dimensionless pressure of equation (14) may be rearranged to yield the intruded cross-sectional area of the dislocation as

$$a \approx \frac{\pi l^2 (p - p_s) k}{e^{-1} c \mu} \quad (42)$$

where it is assumed that the ratio  $k/\mu$  is independently available. Since  $U_D$  cannot be independently determined in this regime, the propagation velocity,  $U$ , remains indeterminate, but a lower bound may be established as  $U_{\min}$ , since  $U_D > 10^0$ .

#### Point Dislocation for $U_D < 10^{-1}$

If early pressure rise in the prepeak pressure regime is well defined in the data, a unique fit should be possible, enabling  $U_D$  to be explicitly determined. Providing a match point at  $U_D(t_D - t_\beta) = 10^0$  enables the minimum distance,  $l$ , to the dislocation to be determined from equation (40). Again, if the geometry of intrusion is well defined, then diffusivity may be independently verified. With  $l$  defined and  $U_D$  available explicitly from the curve match, dislocation velocity may be evaluated from equation (15). The unique peak magnitude of pore pressure in this regime of  $P_\beta = 10^0$  enables cross-sectional area,  $a$ , to be evaluated from equation (14).

#### Line Dislocation for $U_D > 10^0$

Similar to the response for the point dislocation, a single data set allows multiple fits due to the similarity in the response curves. All selected curves for  $U_D$  possess a unique match point value of  $(t - t_\beta)$ , although the product  $U_D(t - t_\beta)$  remains constant. The separation length between the dislocation and the measurement location may be evaluated from equation (40), leaving the dislocation width,  $w$ , to be evaluated.

Dislocation width may be evaluated on noting the linear dependence of peak pressure magnitude,  $P_\beta$ , on dimensionless penetration rate,  $U_D$ , in Figures 10 and 11. The time to peak pressure response,  $x_\beta$ , may be determined from equation (39) where, for large  $U_D$ ,  $U_D \approx x_\beta \approx R\beta$  and equation (37) reduces to

$$U_D P_\beta \approx \sqrt{\frac{\pi}{2}} e^{-1/2} \approx 0.7602. \quad (43)$$

From this the cross-sectional width,  $w$ , may be determined directly as

$$w \approx \frac{\sqrt{2\pi} l (p^1 - p_s) k}{e^{-1/2} c \mu} \quad (44)$$

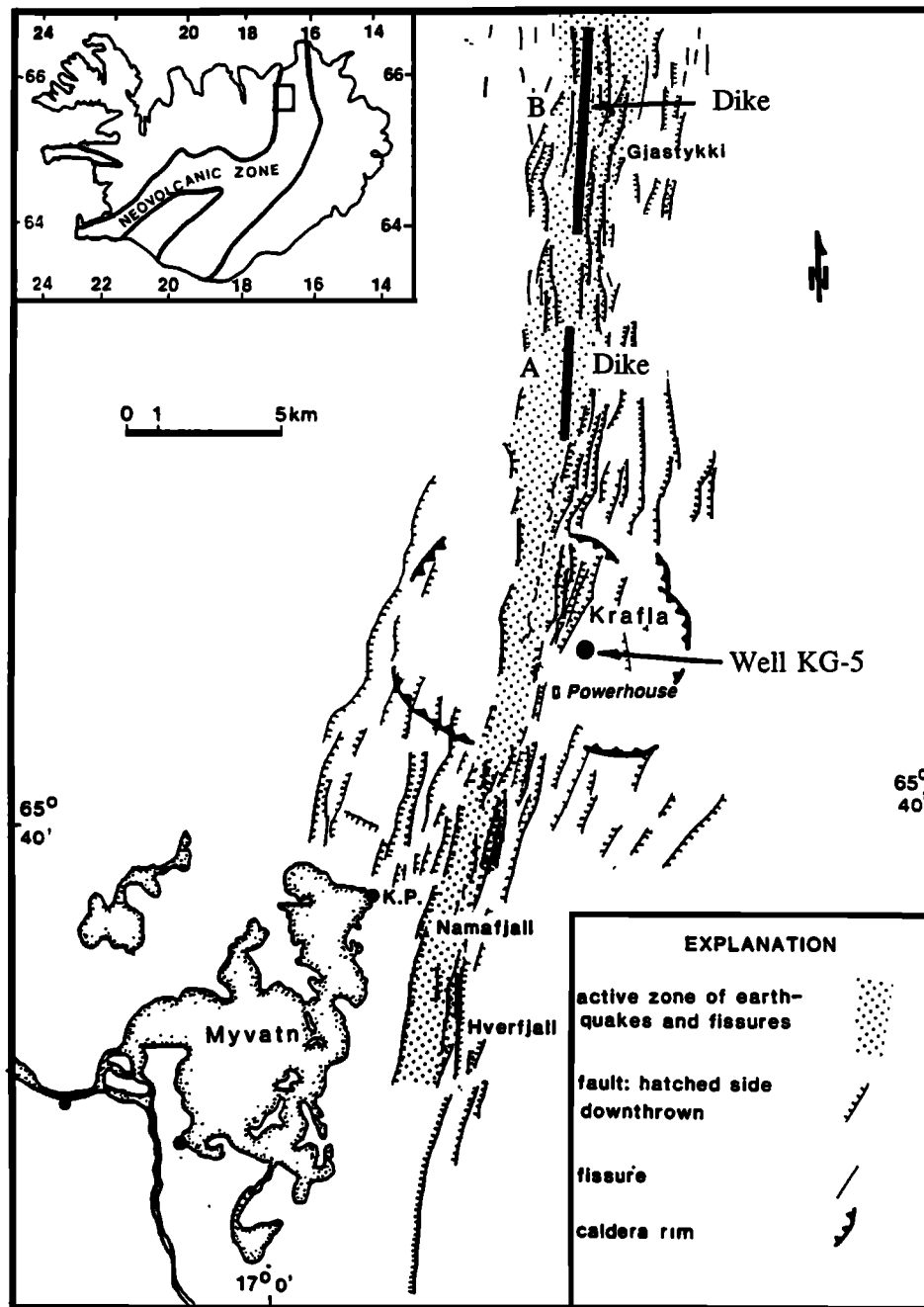


Fig. 12. Outline map of Krafla volcanic system. Caldera rim encloses magma storage chamber. Intrusions are concentrated in fissure swarm. Observation well is 1 km NNE from powerhouse. Eruption associated with September 1977 event occurred at A, and intrusion event of July 1978 occurred at B in southern Gjástykkí. Fissures after K. Saemundsson (unpublished data, 1991). Figure after Ewart *et al.*, [1990].

although  $U_D$ , and hence true intrusion velocity,  $U$ , remains indeterminate. However, a lower bound may be established for the intrusion rate,  $U_{\min}$ , since  $U_D \geq 10^0$ .

#### Line Dislocation for $U_D < 10^{-1}$

The unique form of the various pressure response curves enables  $U_D$  to be determined directly. From the match point in time, the length,  $l$ , may be determined explicitly if hydraulic diffusivity,  $c$ , is known a priori. Real intrusion or penetration rate may be recovered from the dimensionless intrusion rate of equation (15) and dislocation width evaluated from the unique

relation,  $P\beta = -\ln(U_D)$ , through equation (35). This form may be obtained on noting that for small  $U_D$ ,  $x_D \rightarrow 0$  and, consequently,  $R_D = 1$ . The limiting form for large  $x$  of the modified Bessel function is  $K_0[x] \approx -\ln(x)$ . Consequently, location, dislocation velocity, and injected volume may be determined.

#### KRAFLA DATA

Pore pressure data documenting magmatic intrusions are rare, but data for several separate dike intrusions are available for Krafla, Iceland, as reported by Sigurdsson [1982]. The pressure pulses are recorded in a single open observation well, KG-5,

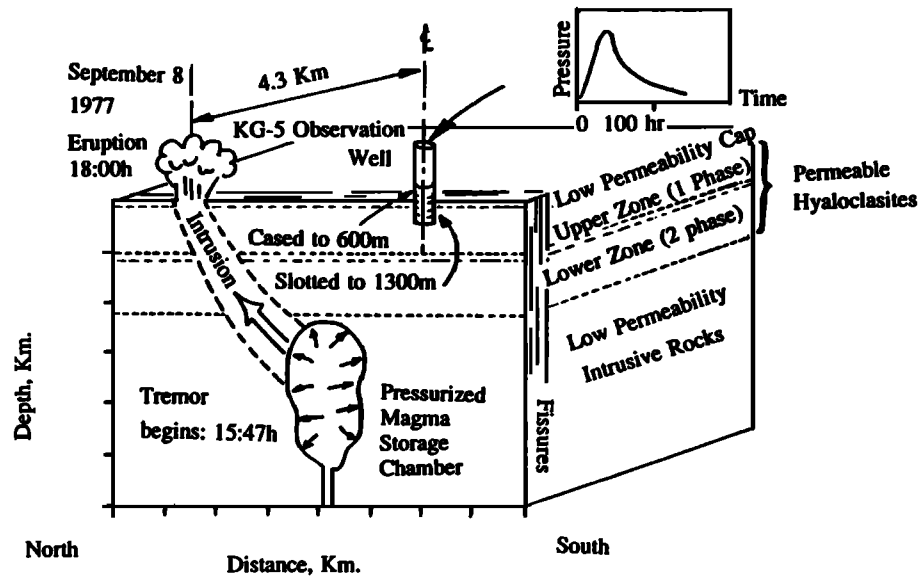


Fig. 13. Block diagram aligned along the Krafla fissure swarm showing the magma intrusion system, the September 8 eruption site and observation well KG-5. Wellfield geologic setting indicated on the south face.

completed to 1300 m and cased to a depth of 600 m. The two magmatic events (sheet intrusions) occurred on September 8, 1977 and July 10, 1978, and are identified by documented peak pressure increases ( $p^p - p_s$ ) in well KG-5 of 0.76 MPa and 0.34 MPa, respectively. The separation between the recording well and the surface phenomena associated with the two events was 4300 m for the September event and about 9300 m for the July event, as illustrated in Figure 12. An eruption occurred in the September event [Saemundsson, 1991].

The site geology comprises lower and upper geothermal reservoirs, with interaction retarded by a confining bed [Stefánsson, 1981]. Well KG-5 terminates in the upper single phase reservoir (liquid dominated with a mean water temperature of 205°C) while the intrusive events, initiating from a magma chamber below 3-km depth [Ewart et al., 1990], affects also the lower two-phase reservoir (liquid-vapor with a mean temperature of 300°C-350°C). Pressure transients have not been detected in wells connected only with the lower zone. A schematic diagram indicating the form of the September 1977 event is shown in Figure 13. Sigurdsson [1982] used the early pressure response of the two intrusive events in a stationary conceptual model to evaluate the permeability and storage coefficients for the reservoir. The model enabled the product of permeability and reservoir height (transmissivity= $kh/\mu$ ) and the product of storage and reservoir height (storativity= $kh/(\mu c)$ ) to be determined for the upper reservoir: transmissivity of  $8.1 \times 10^{-9}$  to  $16.8 \times 10^{-9}$  m<sup>3</sup>/Pa s and storativity of  $2.1 \times 10^{-11}$  to  $3.7 \times 10^{-11}$  m/Pa. Production tests for the upper reservoir [Sigurdsson, 1982; Table VI] yield the following: transmissivity of  $6.0 \times 10^{-9}$  to  $18.3 \times 10^{-9}$  m<sup>3</sup>/Pa s and storativity of  $0.85 \times 10^{-11}$  m/Pa. Likewise, well test data by Bodvarsson et al. [1984] suggest transmissivities averaging about  $6.6 \times 10^{-9}$  m<sup>3</sup>/Pa s for both upper and lower reservoirs with upper reservoir transmissivity for hole KG-9 (closest to KG-5) about  $13.2 \times 10^{-9}$  m<sup>3</sup>/Pa s. Bodvarsson et al. [1984] report no storativity values applicable to the upper reservoir. The following field data are selected for the dislocation model based on field tests: transmissivity of  $6.6 \times 10^{-9}$  to

$13.2 \times 10^{-9}$  m<sup>3</sup>/Pa s representing the "wellfield average" and "nearest well" analyses [Bodvarsson et al., 1984] and storativity of  $0.85 \times 10^{-11}$  m/Pa from the reservoir tests of Sigurdsson [1982]. From these data the hydraulic diffusivity ( $c = \text{transmissivity/storativity}$ ) is calculated as 234.5 to 469 m<sup>2</sup>/s and the permeability,  $k/\mu$ , as  $1.09 \times 10^{-11}$  to  $2.18 \times 10^{-11}$  m<sup>2</sup>/Pa s. These values are summarized in Table 1. Estimates of reservoir height,  $h$ , used in these calculations are of the order of 600 m. Data fits may therefore be attempted with each of the two events. Pressure rise data for the two events are plotted relative to time to peak pressure ( $t - t^p$ ) in Figures 14 and 15 for pressure rise and decline portions, respectively.

Event of September 8, 1977

The line and sheet dislocation models are applied to a sheet intrusion of limited length that pressurized the upper reservoir as it broke to the surface north of the magma storage area. The steepness of the pressure rise, apparent in Figure 14, suggests a fit with the point dislocation solution for  $U_D > 10^0$ . The data for this event are shown superimposed on the appropriate type curves in Figures 16 and 17 for prepeak and postpeak data, respectively. Following the procedure described in the preceding section, the ambiguous match point for  $U_D(t_D - t_D^p) = 10^0$  gives the unambiguous magnitude of  $U_D(t - t^p) = 2.2 \times 10^4$  s. An almost perfect fit is achieved. Substituting this magnitude and the magnitudes of hydraulic diffusivity estimates from Table 1 into equation (30) enables the minimum distance to the measuring location,  $l$ , to be

TABLE 1. Hydraulic Parameters for the Krafla Geothermal Field

Parameter	Magnitude	Units
Hydraulic diffusivity, $c$	7.73-15.47 × 10 <sup>2</sup>	m <sup>2</sup> /s
Permeability, $k/\mu$	1.09-2.18 × 10 <sup>-11</sup>	m <sup>2</sup> /Pa s

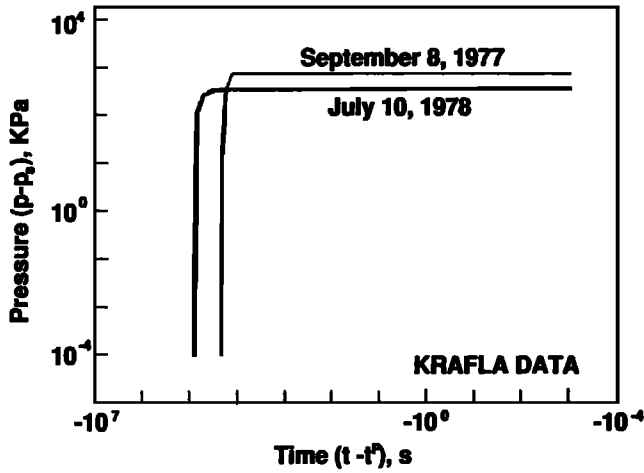


Fig. 14. Transient pore fluid pressure response measured in wellbore KG-5 at Krafla in the prepeak pressure regime.

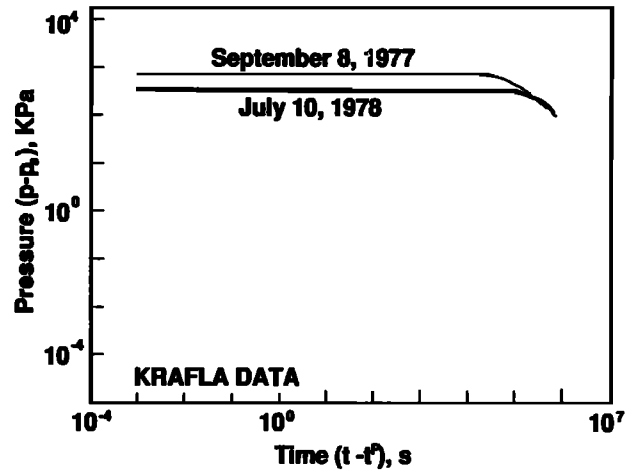


Fig. 15. Transient pore fluid pressure response measured in wellbore KG-5 at Krafla in the postpeak pressure regime.

determined as  $l = 4123$  to  $5834$  m. This compares favorably with the distance to the eruptive event reported as  $4300$  m previously. With this length range determined, the cross-sectional area of the dislocation may be evaluated from equation (42) as between  $0.71$  and  $5.72$   $m^2$ , where the permeability and diffusivity estimates reported in Table 1 are used. This, however, is difficult to reconcile with a dike  $700$  m long and about  $70$  cm wide.

As noted previously, no estimate of the dislocation velocity is possible. A lower bound may, however, be applied on noting from the form of the type curves (Figure 5) that  $U_D > 10^0$ ;

therefore the minimum velocity is found to rest between the bounds  $U_{min} = 0.265$  to  $0.750$  m/s. This range compares favorably with  $U = 0.4$  m/s, as reckoned from magma ascent along an inclined  $4.5$ -km path in  $193$  min [data from *Brandsdóttir and Einarsson, 1979*]. Results are reported in Table 2.

A reasonable but slightly less conclusive match is also made with the model for a sheet intrusion. The ambiguous match point for  $U_D(t_D - t^p) = 10^0$  gives the unambiguous magnitude of  $U_D(t - t^p) = 1.2 \times 10^3$  s. From this, equations (40), (44) and the relation  $U_D > 10^0$  may be used to yield  $l$ ,  $w$ , and  $U_{min}$ .

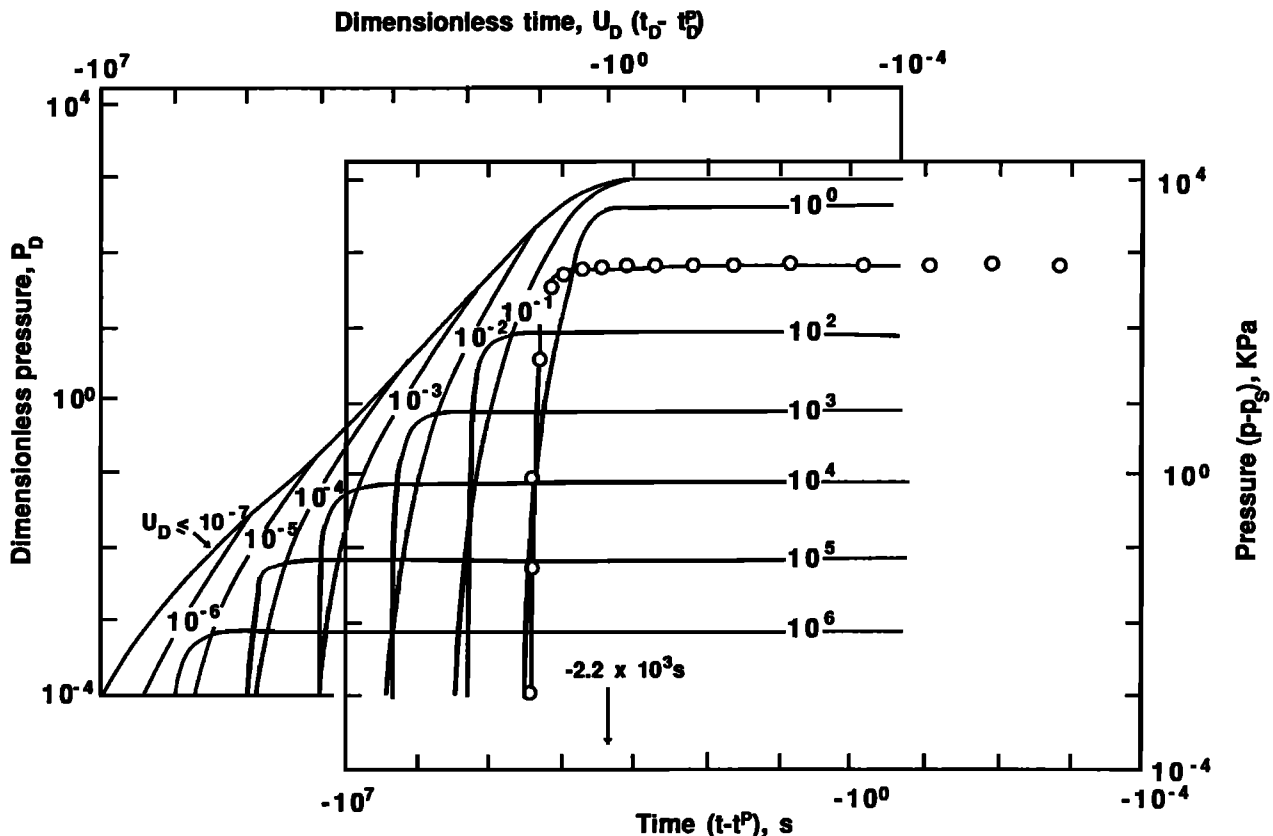


Fig. 16. Prepeak pressure data for the event of September 8, 1977 superimposed on the type curve for a line dislocation.

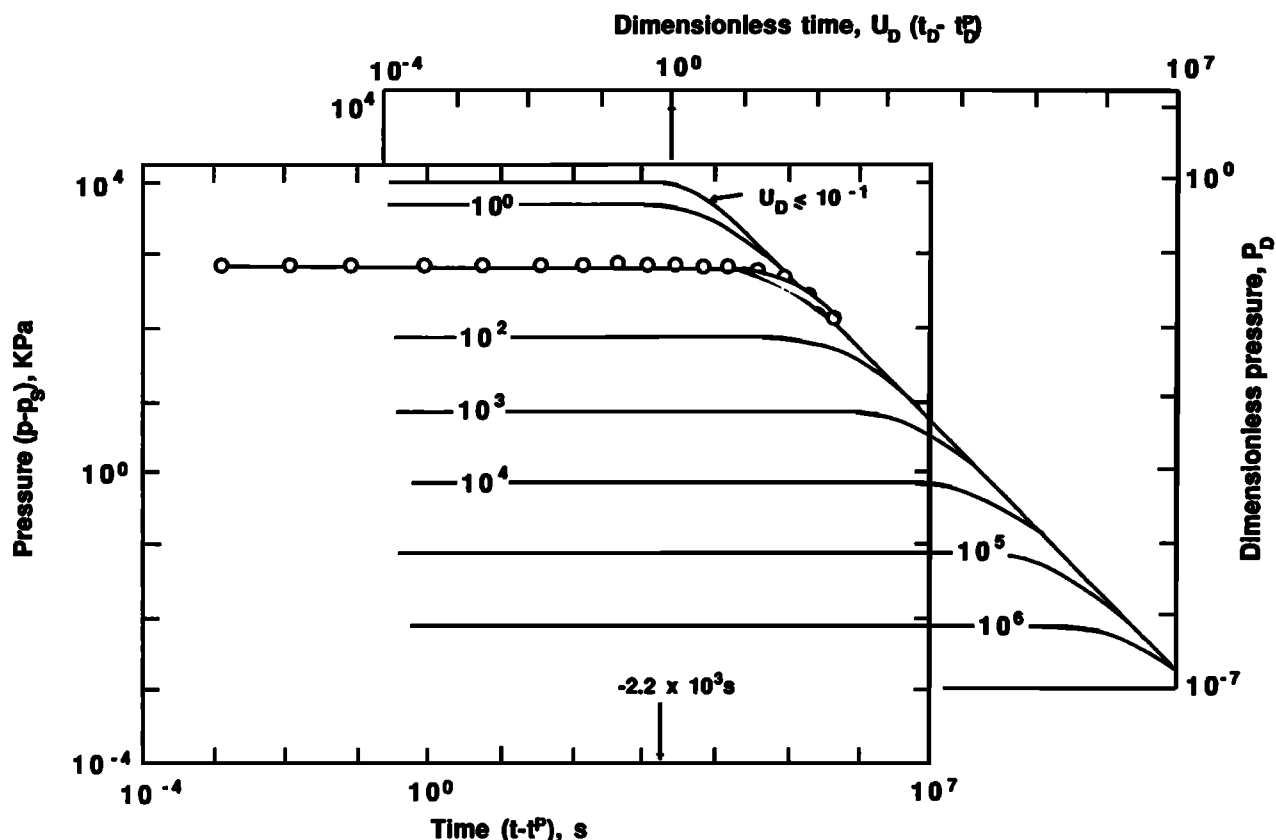


Fig. 17. Postpeak pressure data for the event of September 8, 1977 superimposed on the type curve for a line dislocation.

respectively. These magnitudes are documented in Table 3 for comparison.

Event of July 10, 1978

In this event, distance measurements show that magma was emplaced as a dike in southern Gjástykki, roughly 10 km north of the borehole; surface widening in this zone was measured to be 1 m wide at the surface [Tryggvason, 1980]. The northern extent of magma has not been determined. The procedure for the September event may be repeated where the appropriate unambiguous match corresponds to  $U_D(t-t^p)=10^5$  s for the line dislocation. From this the length separation, cross-sectional area, and minimum dislocation velocity ranges are evaluated as 8792 to 12,437 m, 1.45 to 11.62 m<sup>2</sup>, and 0.124 to 0.352 m/s, respectively. These evaluated parameters are summarized in Table 2 for both events. Notably, for this event, the separation length corresponds well with the reported separation between borehole KG-5 and the center of seismic activity at 9300 m, as reported by Sigurdsson [1982]. Once again, however, the

cross-sectional area seems unreasonably small compared to any physically reasonable value for a dike kilometers long and one meter wide.

Although independent estimates of minimum advance rate,  $U_{min}$ , are not available, the estimates presented in Table 2 appear plausible. The satisfactory agreement between predicted and measured response further suggests that a moving point dislocation provides, in some respects, an adequate physical representation of the process of dike emplacement.

Matching the data of this event with the model for a sheet dike yields, for  $U_D(t_D-t_D^p)=10^0$ ,  $(t-t^p)=1.2 \times 10^3$  s. Using the same procedure as previously, the parameters illustrated in Table 3 are obtained.

CONCLUSIONS

A theory is developed to represent the process of intrusion in a saturated porous elastic solid by a continuous moving point dislocation. The process is assumed to be displacement controlled and analogous to insertion of a continuous

TABLE 2. Parameter Estimates for Intrusive Events at Krafla using the Model of a Moving Cylindrical Intrusion

Parameter	Sept. 8, 1977	July 10, 1978	Units
Length to dislocation, l	4123-5834	8792-12437	m
Cross-section area, a	0.71-5.72	1.45-11.62	m <sup>2</sup>
Minimum velocity, $U_{min}$	0.265-0.750	0.124-0.352	m/s

TABLE 3. Parameter Estimates for Intrusive Events at Krafla using the Model of a Moving Planar Intrusion

Parameter	Sept. 8, 1977	July 10, 1978	Units
Length to dislocation, l	6091-8617	11796-16687	m
Intruded thickness, w	1.36-7.63	2.35-6.61	$\times 10^{-4}$ m
Minimum velocity, $U_{min}$	0.179-0.508	0.093-0.262	m/s

volumetric dislocation at constant rate. Attention is restricted to the pore fluid pressures induced as a result of the intrusion. The full transient behavior for pressure rise and subsequent dissipation is represented. A quasi-steady approximation to this behavior, however, appears adequate in representing the important aspects of behavior as recorded at a static monitoring location as the dislocation passes. This procedure enables the transient pore pressure behavior to be conveniently recorded in terms of dimensionless pressure,  $P_D$ , as a unique function of dimensionless intrusion velocity,  $U_D$ , and dimensionless time,  $t_D$ . To be useful in analyzing field data the transient response is most conveniently described relative to a field discernible landmark in time such as time of initiation, passage or arrest. The most applicable parameter in this analysis is dimensionless time to peak pressure,  $t_D^*$ , and this is used in the analysis.

When plotted relative to time to peak pressure, the transient pressure response for a moving point dislocation exhibits separate families of behavior representing slow and fast intrusion. For slow intrusion the pressure transient record relative to time to peak is symmetrical, reflecting the near-spherical symmetry of the induced pressure bulb relative to the advancing dislocation front. As the dimensionless intrusive velocity is increased, the response develops an increasing asymmetry in both time and space (relative to the dislocation front). The pore pressure contours ahead of the front are compressed resulting in the pressure rise becoming considerably more rapid than the decay. This transition in behavior is observed as intrusion rate,  $U_D$ , increases through unity isolating separate behaviors for  $U_D < 10^{-1}$  and  $U_D > 10^0$ .

The two different responses enable different parameters describing the intrusive event to be determined. Assuming that the hydraulic parameters of permeability,  $k/\mu$ , and diffusivity,  $c$ , representing the host porous medium are known a priori, then the full set of parameters representing the dislocation path,  $l$ , dislocation velocity,  $U$ , and dislocation cross-sectional area,  $a$ , may be recovered. Where the geometry of the intrusion is defined, hydraulic diffusivity of the host,  $c$ , may be determined in lieu of the length to the dislocation,  $l$ . For the slow dislocation, all three of these important parameters may be determined. However, for the fast dislocation, only a minimum advance rate may be recovered. Irrespective of this slight deficiency, the technique offers a potentially important resource in representing and characterizing intrusion from pressure transient records, subject to the limitations of the simplified conceptual model. Indeed, a surprising wealth of information is available purely from this pressure transient record.

A number of assumptions are important in simplifying the process of intrusion to a tractable form. It is assumed that the intrusive event progresses at a continuous rate, develops negligible shear stresses at the interface, that the fluid diffusive process remains isothermal, and that the volume of intruded solid dominates over the potential steam flash volume generated at the contact between the magma and the saturated host rock. Actually, the requirement that fluid diffusion progresses in a strictly isothermal environment may be relaxed, providing non isothermal transport is purely diffusive. A hot source will create an additional fluid pressure increase, exhibiting a similar transient dependence to the pressure transient record. As a consequence, the transient record may be incorrectly interpreted to result from a spuriously large dislocation volume or as indicative of a porous medium represented by a decreased hydraulic diffusivity,  $c$ .

Although the analyses for moving dislocations are introduced

in transient form, as illustrated in equation (19), the reduction of data is completed using a steady approximation of these fully transient systems. The validity of using the steady approximation may be checked. For the Krafla data, appropriate values of the parameter  $U_D x_D$  are of the range 1 to 3 for the 1977 and 1978 events, respectively. Equation (27) reduces to  $Ut=R$ , where  $R$  is the radius to which the steady state has migrated (pore pressure is 95% of the steady magnitude) after time  $t$ . For a dislocation moving at velocity  $U=0.5$  m/s, and for time to peak pressure from the initiation of the eruption as  $10^4$  for 1977 and  $10^5$  for 1978, then migration radii,  $R$ , are 5000 m and 50,000 m for the 1977 and 1978 events, respectively. Since these dimensions are of the order, or greater than, the separation between dike and measuring location, then the use of a steady state appears reasonable, especially postpeak.

Few field data are available to test this theory but promising correspondence is achieved between the theoretical response and data available for two intrusive events at Krafla, Iceland. The calculated cross-sectional area,  $a$ , is several orders of magnitude smaller than the actual intrusion cross-sectional area. This mismatch is a result of the observed pore pressures being orders of magnitude smaller than those anticipated from the proposed theory. A number of explanations are possible, although none appear entirely satisfactory.

Since pore pressures are manually measured within the open annulus of a well, the volume compressibility of this measuring system may be sufficiently large to mask the true magnitude of the pore pressure rise. Pore pressure rise within the surrounding formation may be much higher than that transferred to the well through a rise in fluid level. This volume compressibility of the measuring system or wellbore storage effect is a plausible explanation for the mismatch. However, also associated with this mechanism would be an anticipated time lag in the pressure response resulting from the finite time taken for the pore pressures induced around the well to diffuse to the measuring well. The excellent match in intrusion rates and length to the dislocation suggests that the time history of the pore pressure response is not significantly affected.

Alternatively, the deficit in pore pressure magnitudes may result from the competing mechanisms of magma chamber deflation that accompany dike inflation. Pore pressure increases that result from dike emplacement may be countered by pore pressure decreases that result from concurrent deflation of a shallow magma chamber that is close to the measuring well. In this, the deflation and inflation components would, by definition, be simultaneous, with the net effect that the transient pore pressure response would be minimally shifted in time. An unattractive feature of this explanation, however, is that the magma chamber resides within the two phase reservoir through which pressure pulses are poorly transmitted.

The reservoir comprises imperfect elastic material, with fractures cutting the upper aquifer and sometimes passing into the overlying bed. The effect of this would be to enable pore pressure pulses in open fractures to dampen the total stress and pore pressure pulses. The effect of a cracked aquifer would reduce the total stress field magnitude at any arbitrary distance of the wellsite from the intrusion. The overall effect would be to induce pore pressures in the far field much lower than theoretical values, but not to greatly influence the time history of the pulse. Similarly, the presence of strain dependent moduli or modulus anisotropy in the aquifer rock mass, as a result of tectonic influences, may result in the effective dampening of the pore pressure pulse.

A final explanation of the mismatch in the pressure response may be the fact that the intrusions at Krafla were dikes obliquely oriented to the observation well and not cylindrical intrusions as assumed in the theory. The dikes had lengths on the order of 1 km and exhibited separation of about 1 m. Apparently, when such sheet-like features of limited length are viewed from a highly oblique position (nearly along strike), they can behave, in some respects, as if they were propagating point dislocations of relatively small effective cross-sectional area. The point volumetric dilation centers used in this analysis do not truthfully replicate the shear-stress-free conditions that may prevail at the interface between the viscous dike and the host rock. This shortcoming of the model is particularly apparent when the measuring location is oblique to the dislocation, as a zone of partial dilation is not adequately represented.

Despite the mismatch in measured and predicted pressure magnitudes, the separation distances and advance rates, calculated primarily from the pressure history data, appear eminently reasonable. The fidelity of the fit between measured and predicted responses is clearly encouraging.

*Acknowledgments.* Data on Krafla well measurements were generously provided by Valgardur Stefánsson of the National Energy Authority of Iceland. Kristjan Saemundsson and Axel Björnsson, of the same organization, provided important logistical support and guidance to B.V. during field studies of the geology and geophysics of Krafla. The support of the National Science Foundation under grants MSM-8708976 to D.E. and BCS-8904990 to B.V. is gratefully acknowledged. The helpful comments of reviewers Paul Delaney and Allan Rubin contributed to the final manuscript.

#### REFERENCES

- Bodvarsson, G. S., S. M. Benson, O. Sigurdsson, V. Stefánsson, and E.T. Eliasson, The Krafla Geothermal Field, Iceland, 1, Analysis of well test data, *Water Resour. Res.*, 20(11), 1515-1530, 1984.
- Brandsdóttir, B., and P. Einarsson, Seismic activity associated with the September 1977 deflation of the Krafla central volcano in north-eastern Iceland, *J. Volcanol. and Geotherm. Res.*, 6, 197-212, 1979.
- Chadwick, W.W., R.J. Archuleta, and D.A. Swanson, The mechanics of ground deformation precursory to dome-building extrusions at Mount St. Helens 1981-1982, *J. Geophys. Res.*, 93(B5), 4351-4366, 1988.
- Cleary, M. P., Fundamental solutions for a fluid-saturated porous solid, *Int. J. Solids Struct.*, 13, 785-806, 1977.
- Cleary, M. P., Moving singularities in elasto-diffusive solids with application to fracture propagation, *Int. J. Solids Struct.*, 14, 81-97, 1978.
- Delaney, P.T., Rapid intrusion of magma into wet rock: groundwater flow due to pore pressure increases, *J. Geophys. Res.*, 87(B9), 7739-7756, 1982.
- Elsworth, D., Dislocation analysis of penetration in saturated porous media, *J. Eng. Mech. Div. Am. Soc. Civ. Eng.*, 117(2), 391-408, 1991.
- Endo, E.T., D. Dzurisin, and D.A. Swanson, Geophysical and observational constraints for ascent rates of dacitic magma of Mount St. Helens, in *Magma Transport and Storage*, edited by M.P. Ryan, pp. 317-334, John Wiley, New York, 1990.
- Ewart, J.A., B. Voight, and A. Björnsson, Dynamics of Krafla caldera, north Iceland: 1975-1985, in *Magma Transport and Storage*, edited by M.P. Ryan, pp. 225-276, John Wiley, New York, 1990.
- Ida, Y., and M. Kumazawa, Ascent of magma in a deformable vent, *J. Geophys. Res.*, 91(B9), 9297-9301, 1986.
- Kushiro, I., Viscosity, density and structure of silicate melts at high pressures and their petrological applications, in *Physics of Magmatic Processes*, edited by R.B. Hargraves, pp. 93-120, Princeton Press, Princeton, N.J., 1980.
- Rice, J.R., and M.P. Cleary, Some basic stress diffusion solutions for fluid-saturated elastic porous media with compressible constituents, *Rev. Geophys.*, 14(2), 227-241, 1976.
- Rudnicki, J.W., On "Fundamental solutions for a fluid-saturated porous solid" by M.P. Cleary, *Int. J. Solids Struct.*, 17, 855-857, 1981.
- Saemundsson, K., Jarðfraedi Kröflukerfisins, in *Náttúra Mývatns*, edited by A. Gardarsson and A. Einarsson, pp. 24-95, Hid íslenska náttúrufræðifélag, Reykjavík, 1991.
- Shimozuro, D., Future prospect of Volcano geophysics, Kagoshima Int. Conf. Volcanoes Proceedings, pp. 433-436, National Institute for Research Advancement and Kagoshima Prefectural Government, Kagoshima, Japan, 1989.
- Sigurdsson, O., Analysis of pressure pulses resulting from volcanic activity in the vicinity of a well, M.S. Thesis, 75 pp., University of Oklahoma, Norman, Oklahoma, 1982.
- Skempton, A.W., The pore-pressure coefficients A and B, *Geotechnique*, 4, 143-147, 1954.
- Stefánsson, V., The Krafla geothermal field, northern Iceland, in *Geothermal Systems; Principles and Case Histories*, edited by L. Rybach and L.J.P. Muffler, pp. 273-294, John Wiley, New York, 1981.
- Tryggvason, E., Subsidence events in the Krafla area, north Iceland, 1975-1979, *J. Geophys.*, 47, 141-153, 1980.
- Turcotte, D.L., Magma migration, *Annu. Rev. Earth Planet. Sci.*, 10, 397-408, 1982.
- Turcotte, D.L., On the role of laminar and turbulent flow in buoyancy driven magma fracture, in *Magma Transport and Storage*, edited by M.P. Ryan, pp. 103-111, John Wiley, New York, 1990.
- Watanabe, H., Changes in water level and their implication to the 1977-1978 activity of Usu volcano, in *Arc Volcanism: Physics and Tectonics*, edited by D. Shimozuru and I. Yokoyama, pp. 81-93, Proceedings of 1981 Symposium of International Association of Volcanology and Chemistry of the Earth's Interior, Tokyo and Hakone, Terra Scientific Pub. Co., Tokyo, and D. Reidel, Dordrecht, 1981.

D. Elsworth, Department of Mineral Engineering, Pennsylvania State University, University Park, PA 16802.

B. Voight, Department of Geosciences, Pennsylvania State University, University Park, PA 16802.

(Received June 10, 1991;  
revised February 8, 1992;  
accepted March 2, 1992.)